Hemodynamic Analysis of Bifurcated Artery Using Computational Fluid Dynamics

Hemapriya Dhamodaran, B. Shreeram, and C. Li

1 Introduction

1.1 Blood as the Fluid

In this work, blood is assumed to be an ideal fluid in nature. The ideal Newtonian fluid is where high shear rate occurs in large arteries. The simulations were carried out by considering the following material parameters such as density 1000×10^{-6} kg/mm³ and dynamic viscosity of 1000 centipoise for all the cases reported here. The theory of Navier-Stokes equations was used for simulations of the blood flow.

1.2 Geometry Preparation

The various geometry cases for the bifurcated artery configurations created on this platform are listed in Table 1.

H. Dhamodaran (✉)
Department of Medical Physics, Royal Infirmary of Edinburgh, Edinburgh, UK

B. Shreeram
Department of Mechanical Engineering, KGISL Institute of Technology, Coimbatore, India

C. Li
Department of Biomedical Engineering, School of Science and Engineering,
University of Dundee, Dundee, Scotland, UK
e-mail: c.li@dundee.ac.uk

Table 1 Geometry and configuration details of bifurcated artery

Geometry	Configuration	θ_1	θ_2
Case 1	No plaque with bifurcation angles	30°	30°
Case 2	Two plaque configuration 1 without blood clot	30°	30°
Case 3	Two plaque configuration 1 with blood clot	30°	30°
Case 4	Two plaque configuration 2 without blood clot	30°	30°
Case 5	Two plaque configuration 2 with blood clot	30°	30°
Case 6	No plaque with bifurcation angles	30°	45°
Case 7	Two plaque configuration 1 without blood clot	30°	45°
Case 8	Two plaque configuration 1 with blood clot	30°	45°
Case 9	Two plaque configuration 2 without blood clot	30°	45°
Case 10	Two plaque configuration 2 with blood clot	30°	45°

1.3 Meshing

Meshing is the process of breaking down the object into smaller items to define the shape of the object. It is one of the critical steps of the modeling process. With the larger number of elements, an increased accuracy in solution is produced but it takes longer time to process the data. Here, the surface of the shape is to be smoothened to remove the remains of the restoration algorithm. In this simulation, the meshing of the physical object is created by using computer-generated program; the various sizing options including relevance center, smoothing, span angle center, and curvature angles are chosen where plagues are present. Also, fine refinements are carried out in case they are need. Selections are made for the various surfaces and they are named and used for defining the boundary conditions.

1.4 Physics Setup

The physics setup was established considering the steady-state 2D planar flow of an incompressible fluid. The double precision was used, the fluid material was blood with a density of 1000 kg/m³, a viscosity of 0.001, and the velocity was adjusted to get a Reynolds number as 400. The cell zone conditions, for the interior surface, were chosen with the blood as the fluid. Then the boundary conditions for the walls, inner surface, inlet, and outlet were set up with wall, inner surface, velocity inlet, and pressure outlet, respectively, as the type was chosen. This was followed by adding the reference values like density, viscosity, and temperature as 300 K. The solution was initialized by standard initialization and the reference frame was relative to the cell zone that was opted. The initial velocity was set at 1 m/s. The next step is the computation modeling in which the desired solution is generated after several iterative steps. The results show the various display modes for CFD which include the 3D visualization of velocity streamlines, wall shear stress in various boundaries, and pressure contours.

1.5 Fluid Mechanics of Blood Flow

The major characteristics of hemodynamic of any fluid can be realized by analyzing the various related fluid behavioral phenomena. For instance, a study of fluid flow inside conduits provides imminent factors that determine resistance to flow inside blood conduit. Equally, fluid mechanical aspects determine the circulation of fluid stress due to shear acting on the inner side of blood vessels, which has a vital biological consequence.

The most important parameter is the wall shear stress (WSS) [1–9]. WSS is considered carefully as the spatial gradient changes when the dynamic viscosity of the blood acting perpendicular to the blood vessel changes. If the dynamic viscosity of blood is identified, WSS can also be determined.

The stream velocity flow patterns or vector flow patterns are associated with the development of plague formation and progression of the plague before and after vascular interventions. The pressure contours determine an increase in pressure gradient as the bifurcation decreases the flow velocity at that point. By analyzing the above data, the hemodynamic nature of the artery can be studied effectively [10].

2 Contour Analysis

2.1 Velocity Streamline and Pressure Contour

The various factors like shear stress of the walls, streamline, its pressure contours, and velocity are analyzed for the bifurcated artery in all the regions of walls for obtaining the hemodynamic changes and stenosis pathophysiology (Fig. 1).

Case 1: No plaque with bifurcation angles ($\theta_1 = 30°$ and $\theta_2 = 30°$)
The streamline velocity was found to be maximum to about 1.394 ms-1. Due to the bifurcation at the inner wall, the pressure concentration was confined at that point as shown in Fig. 11. The WSS was 14 Pa at the left wall and 10 Pa at the right wall as in Fig. 12. WSS for the left wall was higher than that of the right wall because the diameter of the wall reduces after bifurcation. The pressure contour depicts that there is an increased pressure at the bifurcation point compared to the high-velocity area (Fig. 2).

Case 2: Two plaque configuration 1 without blood clot ($\theta_1 = 30°$, $\theta_2 = 30°$)
A plague was introduced in this case on both the left and the right wall of the artery and this increased the velocity to 1.879 ms^{-1}. Also a recirculation of the blood flow was found near the left walls near the plague due to the thinning of the wall at the bifurcation. The maximum WSS was observed at 26 Pa that was seen on both the right and the left wall initially, but as the distance of the wall on right and left increased towards the outlet, there was a slight dip in the WSS as shown in Figs. 13 and 14. This is because the blood flow had a path to travel after the bifurcation point. The pressure was high near the bifurcation and the dipped lower along the streamline (Fig. 3).
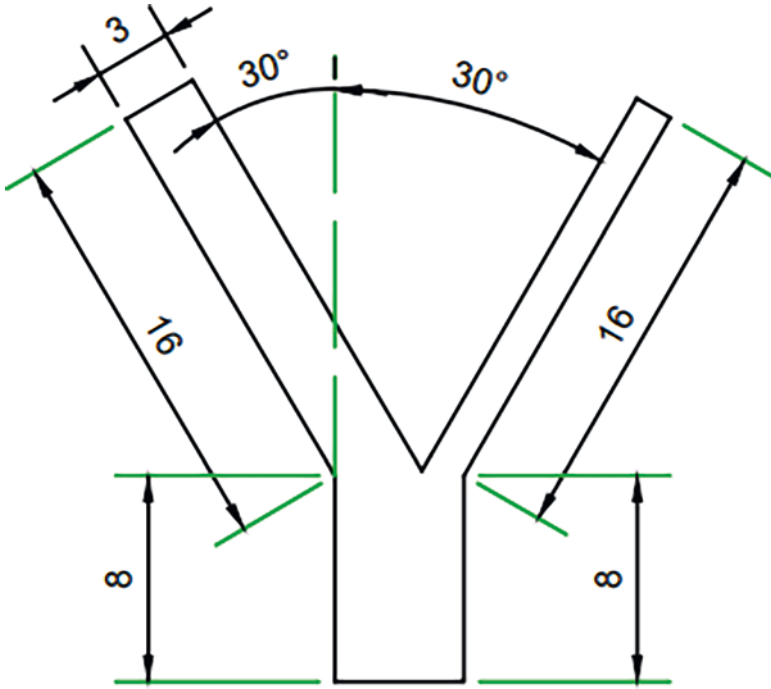
Fig. 1 No Plague ($\theta_1 = 30°$ and $\theta_2 = 30°$)

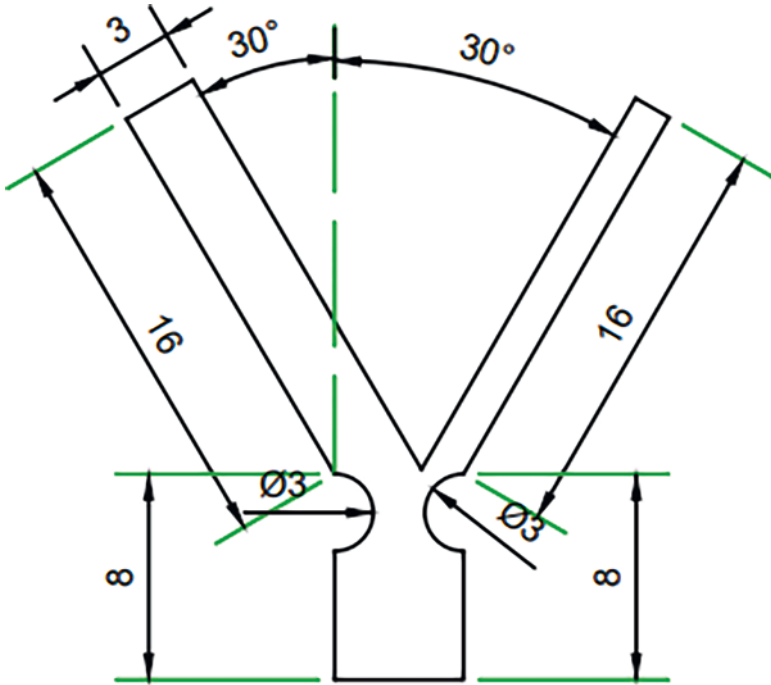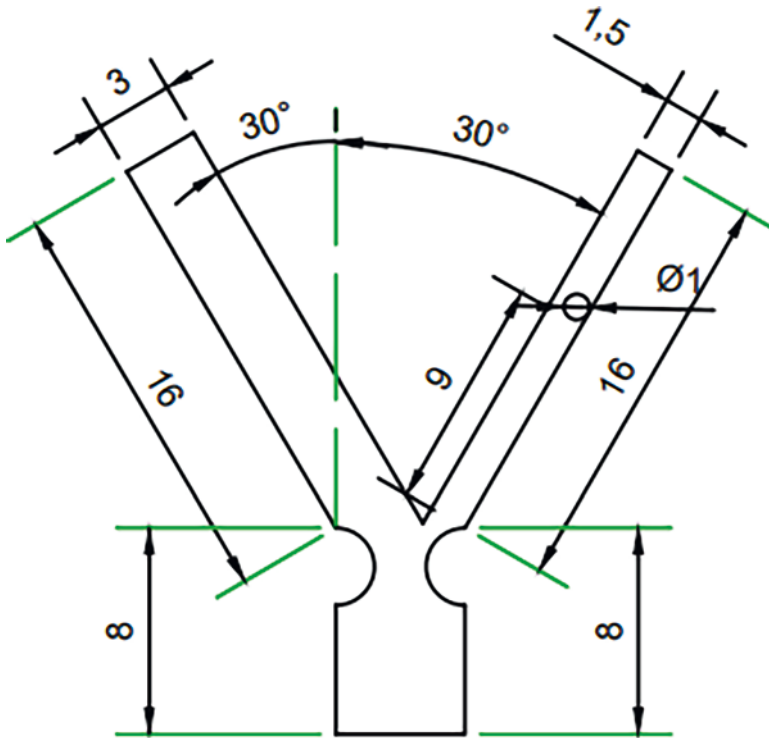**Fig. 2** Two plaque configuration 1 without blood clot ($\theta_1 = 30°$ and $\theta_2 = 30°$)

Fig. 3 Two plaque configuration 1 with blood clot ($\theta_1 = 30°$ and $\theta_2 = 30°$)

Case 3: Two plaque configuration 1 with blood clot ($\theta_1 = 30°$, $\theta_2 = 30°$)
In this configuration, a clot is introduced in the left wall. The maximum streamline velocity was found to increase with the clot to 2.594 ms^{-1}. The streamline velocity increases at the plague and then due to the recirculation of the blood flow, it increases at the right inner wall. When the blood flows with a high velocity near the right wall, it directly bangs the inner right wall; hence, the velocity is found to increase again near the inner right wall. The pressure gradient was found to decrease compared to Case 2. The WSS at the right wall was initially found to be 39 Pa at the first plague, which then increased to 41 Pa at the left wall as in Figs. 15 and 16. But as we go towards the outlet, the right wall had an increased pressure at about 0.015 m in the artery (Fig. 4).

Case 4: Two plaque configuration 2 with blood clot ($\theta_1 = 30°$, $\theta_2 = 30°$)
In this case, three plagues were introduced in which two are in right inner, right outer wall, and one in the left outer wall. Compared to Case 2, the velocity was found to be doubled of 4.537 ms-1. In the left side, the high velocity was found at the region of plague because the artery was thinning out at that point. Also, two recirculation blood flow points were noticed due to the plague geometry; on the
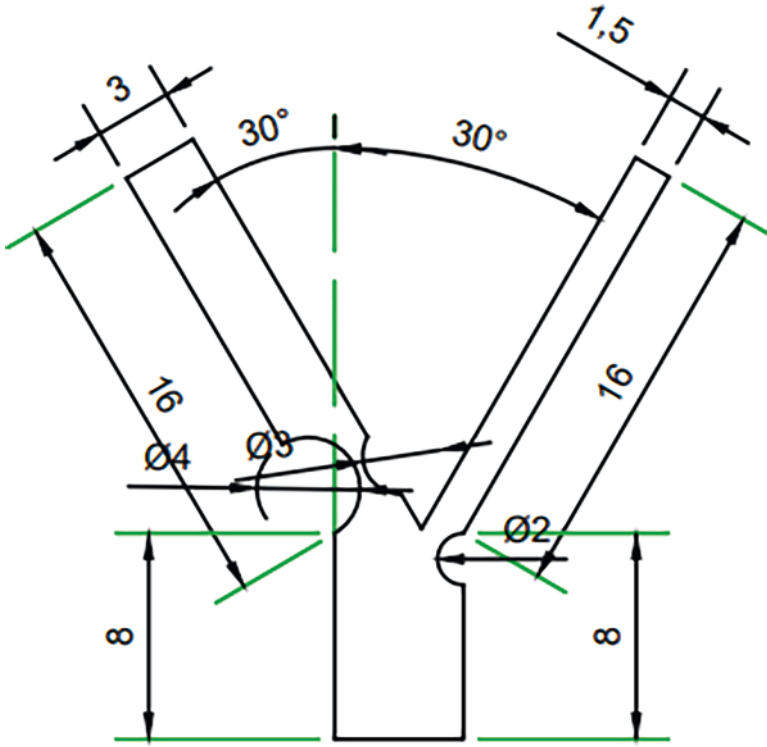
Fig. 4 Two plaque configuration 2 without blood clot ($\theta_1 = 30°$ and $\theta_2 = 30°$)

other hand, the right side bifurcation did not have major change. It had higher velocity at the plague and then the streamline became normal. The pressure was found to decrease compared to Case 2 as shown in Figs. 17 and 18. The WSS was found to increase at the inner wall and it gradually decreased. But the right wall had a high WSS at the beginning and then faded gradually as flow proceeded near the outlet [11] (Figs. 5, 6, 7, 8, 9, 10, 11, 12, 13, 14, 15, 16, 17 and 18).

Case 5: Two plaque configuration 2 with blood clot ($\theta_1 = 30°$, $\theta_2 = 30°$):
In this geometry, a clot was introduced in the left wall same as Case 3 along with a geometry of Case 4. The streamline velocity was found to increase to a maximum of 6.267 ms-1. Due to the clot geometry, there was an increase in the velocity near the clot and near the bifurcation and plaque. The main reason behind this is due to the decline in the diameter of the vein after the plague and clot. WSS overstated to a peak value of 250 Pa at 0.015 m due to the diameter size of the artery that blocks the flow of vessel. The pressure gradient was found to be more at the recirculation part in the left side as there was an increase in the diameter after the plague. This is clearly shown in Figs. 19 and 20.
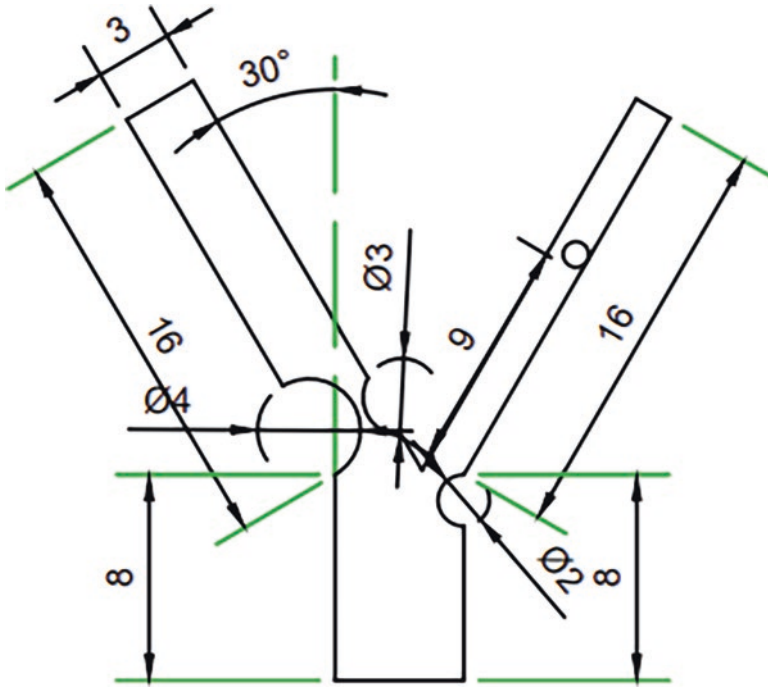
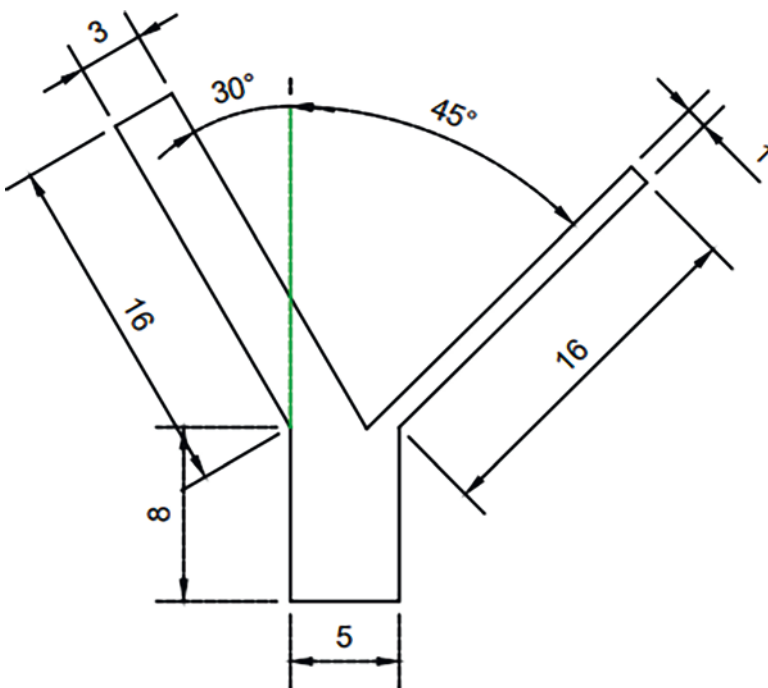**Fig. 5** Two plaque configuration 2 with blood clot ($\theta_1 = 30°$ and $\theta_2 = 30°$)

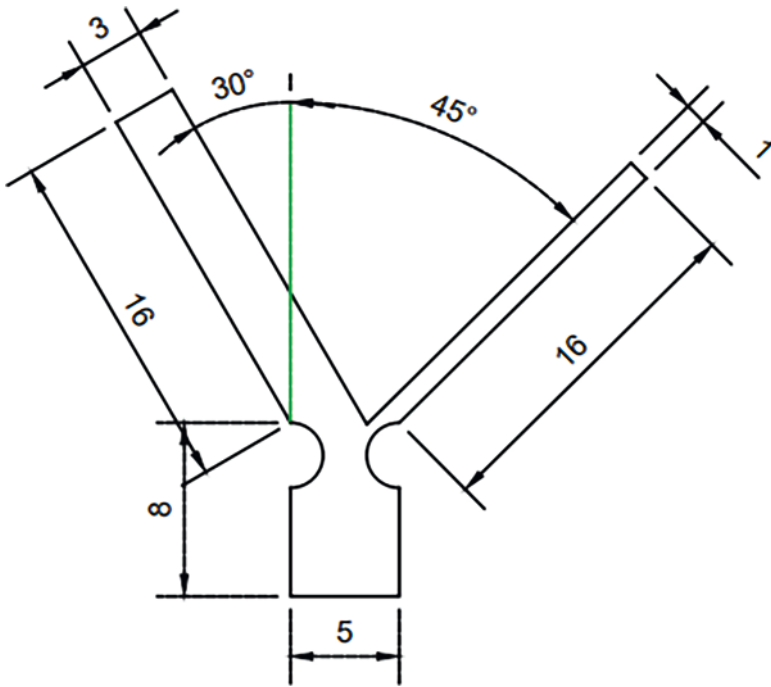**Fig. 6** No plague ($\theta_1 = 30°$ and $\theta_2 = 45°$)

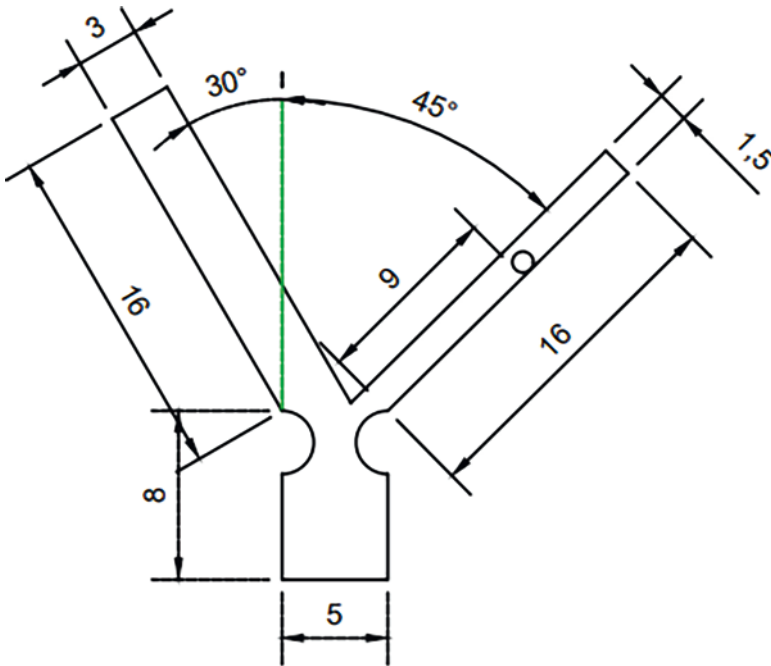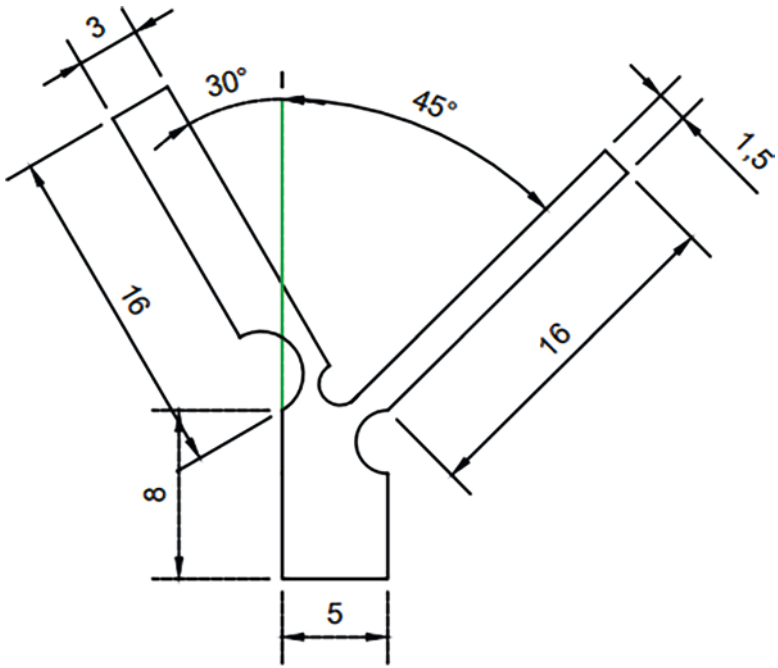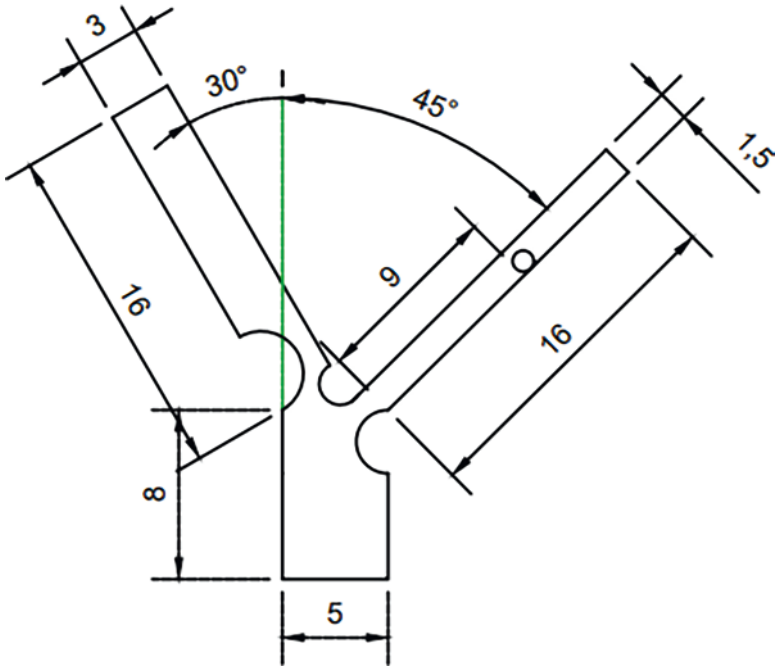**Fig. 7** Two plaque configuration 1 without blood clot ($\theta_1 = 30°$ and $\theta_2 = 45°$)

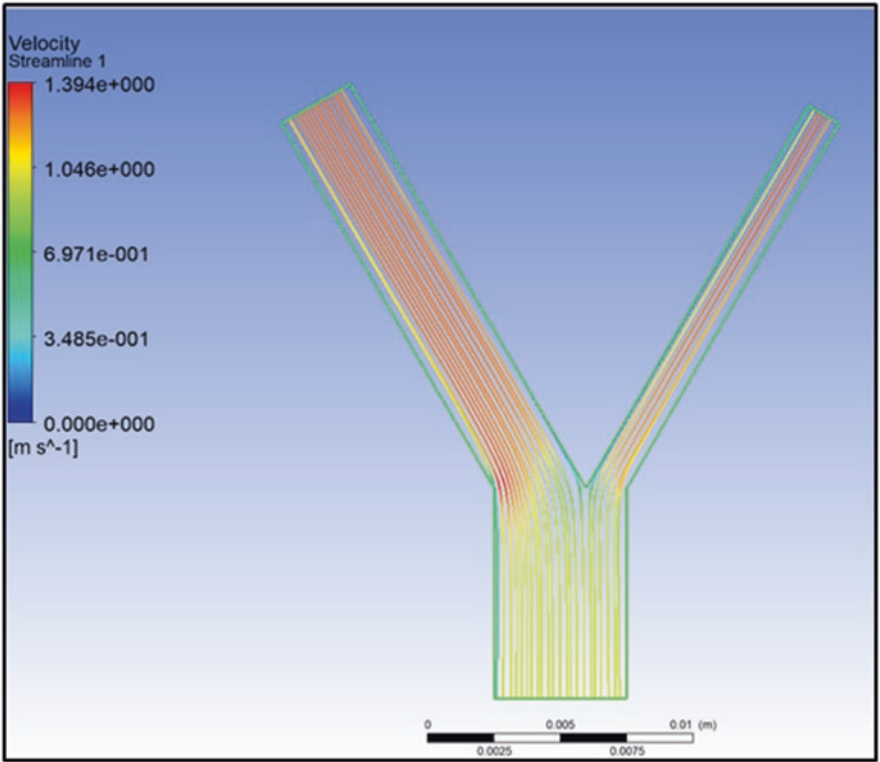**Fig. 8** Two plaque configuration 1 with blood clot ($\theta_1 = 30°$ and $\theta_2 = 45°$)

Fig. 9 Two plaque configuration 2 without blood clot ($\theta_1 = 30°$ and $\theta_2 = 45°$)

Fig. 10 Two plaque configuration 2 with blood clot ($\theta_1 = 30°$ and $\theta_2 = 45°$)

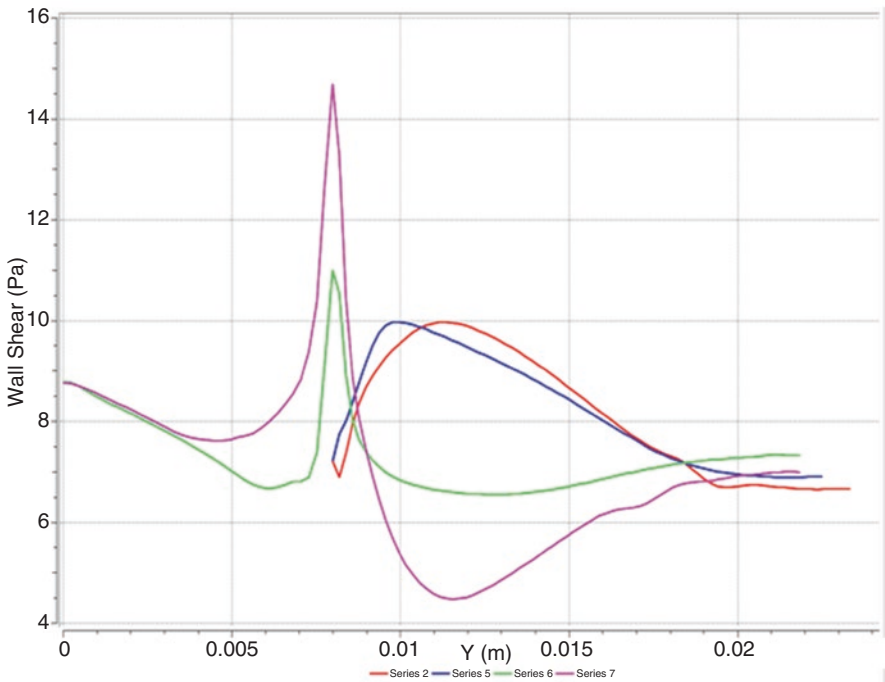**Fig. 11** The velocity streamline curve for Case 1

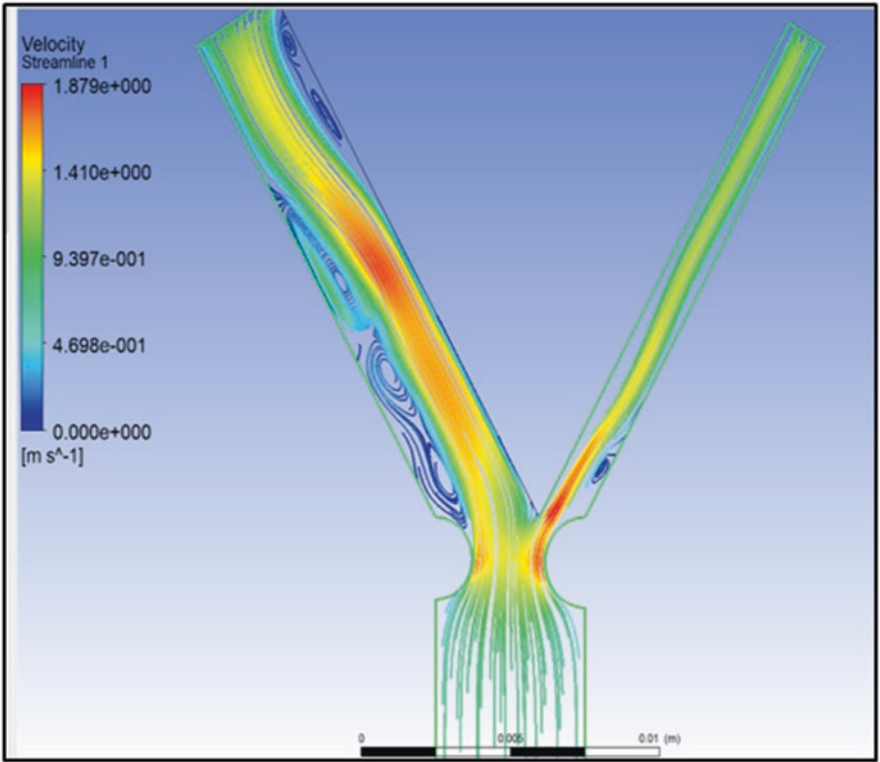**Fig. 12** WSS – various walls for Case 1

Fig. 13 The velocity streamline curve for Case 2
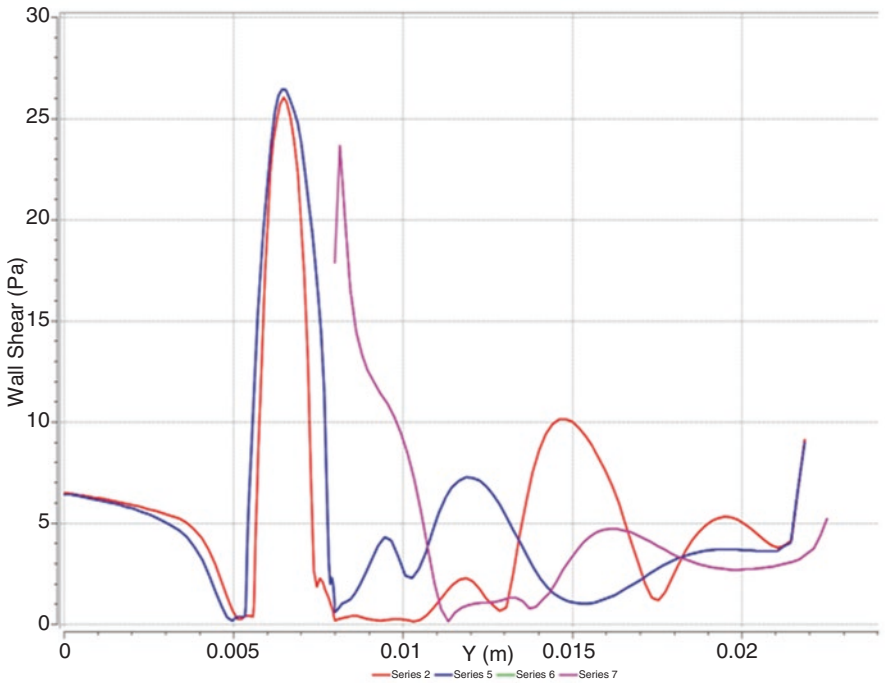

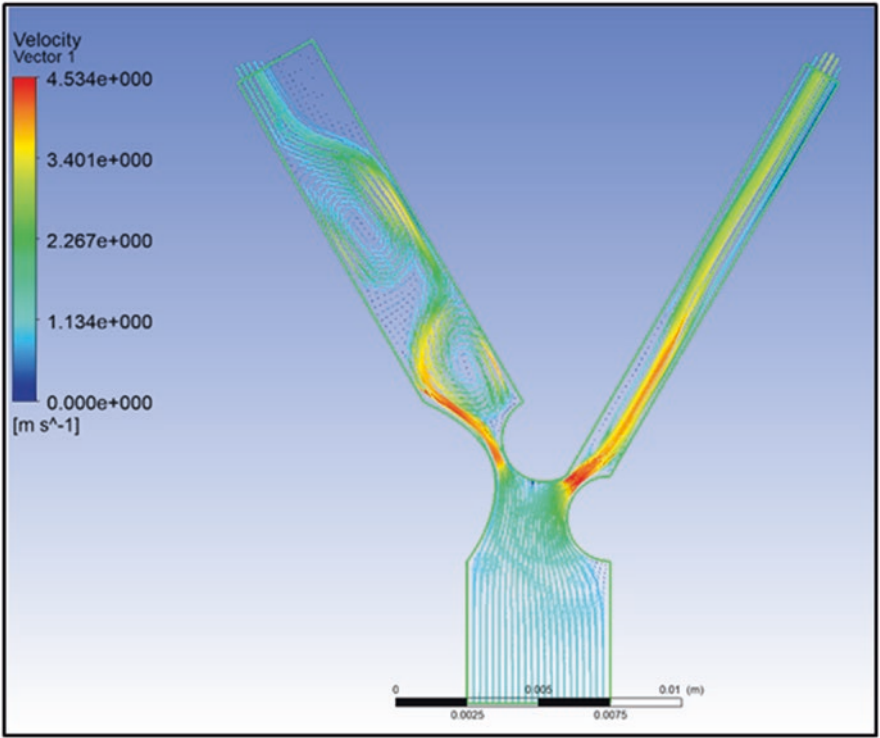**Fig. 14** WSS – various walls for Case 2

Fig. 15 The velocity streamline curve for Case 3
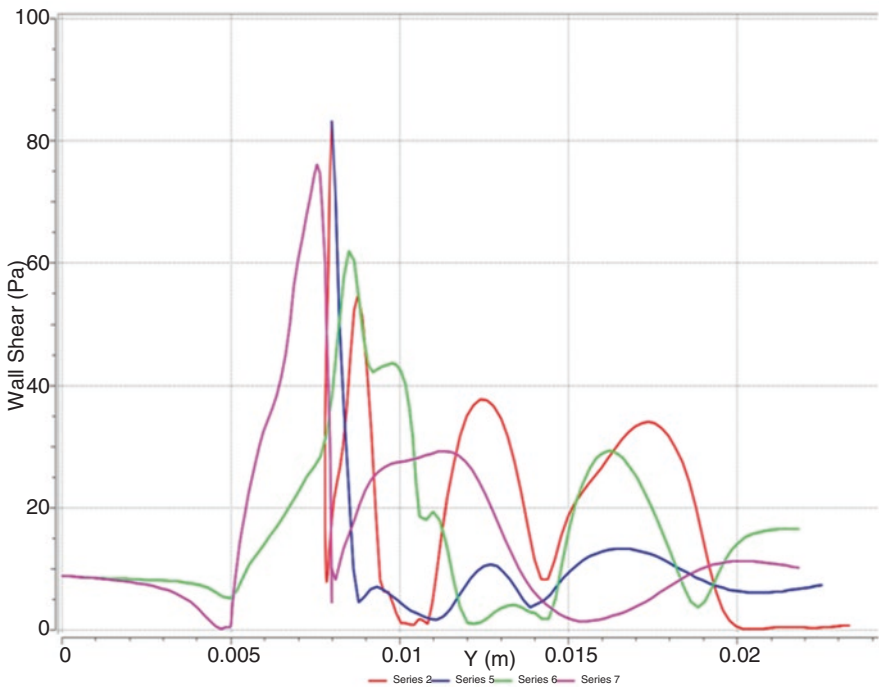

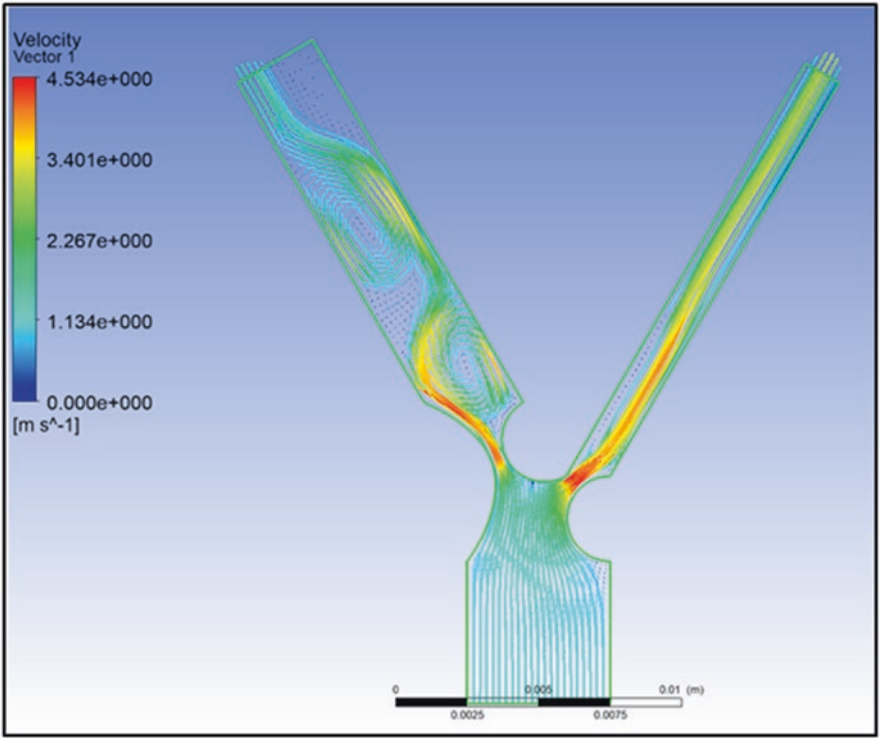**Fig. 16** WSS – various walls for Case 3

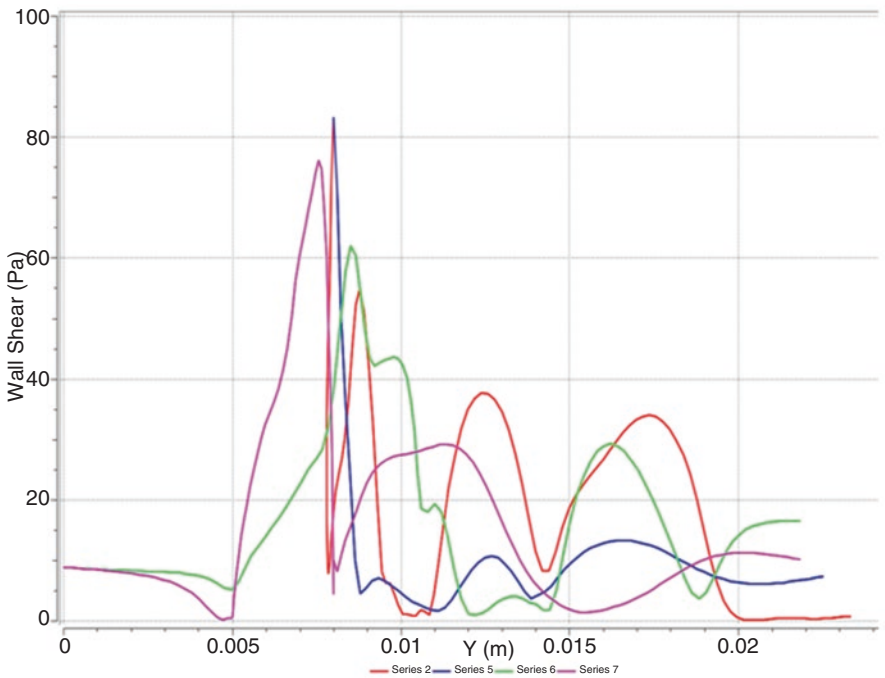**Fig. 17** The velocity streamline curve for Case 4

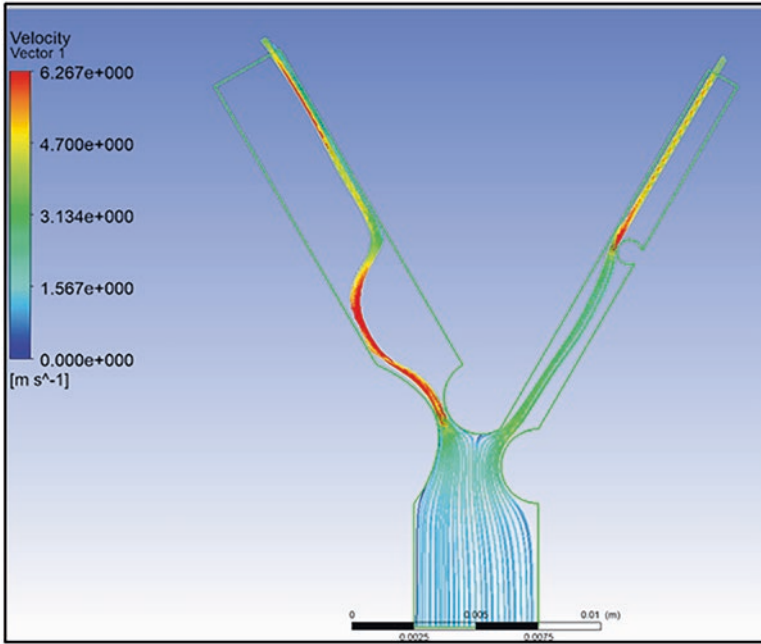

Fig. 18 WSS – various walls for Case 4

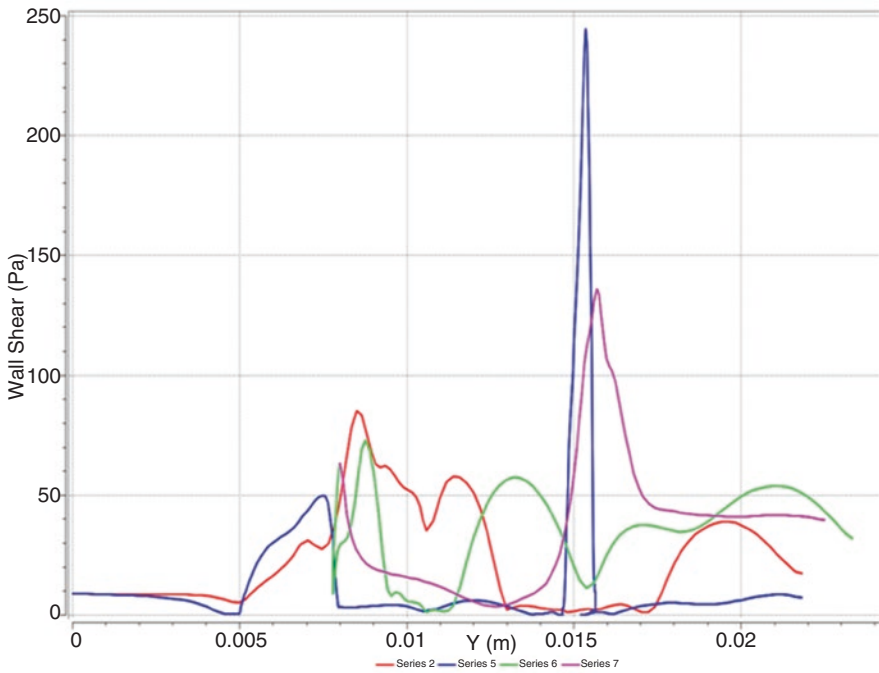**Fig. 19** The velocity streamline and pressure curve for Case 5

Fig. 20 WSS – various walls for Case 5

Case 6: Two plaque configuration ($\theta_1 = 30°$, $\theta_2 = 45°$):
In this case, one of the angles was increased to 45°. This increases the streamline velocity to 1.765 ms^{-1} due to the change in the bifurcation angle. The WSS in the left has 2 peak values of 13 Pa and 10 Pa at 0.0025 m and 0.007 m, respectively; this is due the increase in the curvature in the bifurcation. Also, the right wall has 10 Pa WSS at 0.0025 m. The pressure gradient was seen to be more initially and then it decreased gradually nearing the outlet of both the walls. This is clearly shown in Figs. 21 and 22.

Case 7: Two plaque configuration 1 without blood clot ($\theta_1 = 30°$, $\theta_2 = 45°$):
This is the same as Case 2 but one of the angle was $\theta_2 = 45°$. The velocity was increased just near the plague but as not in Case 2. This is because the blood flow has a curvature which increased the maximum velocity at that point to 1.979 ms^{-1}. The WSS was found to increase the curvature of both left and right walls initially but the velocity towards the outlet in left wall increased after recirculation of the blood flow towards the inner left wall as seen in Figs. 23 and 24. The contour pressure was found to increase in the beginning for the right wall but as we proceed towards the outlet, the pressure dropped.

Case 8: Two plaque configuration 1 with blood clot ($\theta_1 = 30°$, $\theta_2 = 45°$):
This case is the same as Case 3 configuration with a variation in the second angle by 45°. Due to the increase in the bifurcating angle, it was found that the velocity was 2.624 ms^{-1} near the closer end of outlet. The WSS in the left had two peak values of
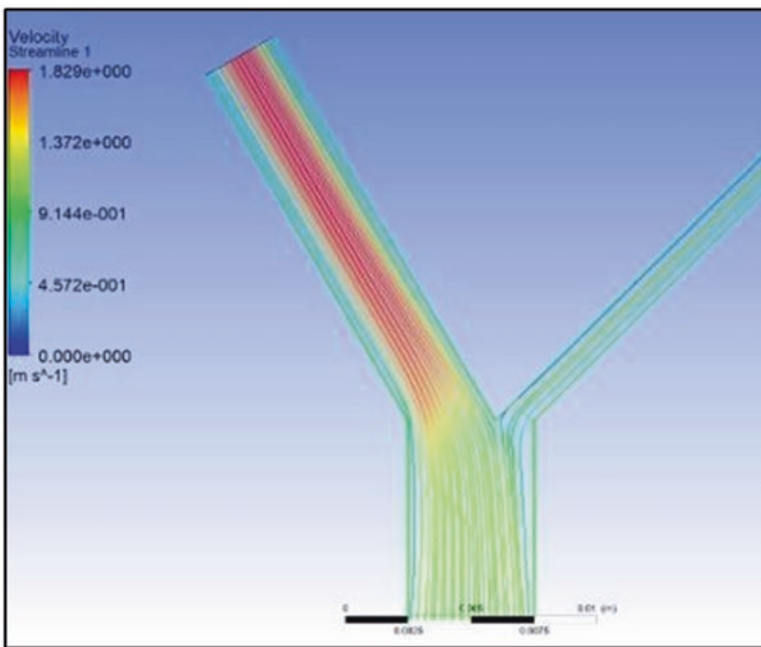

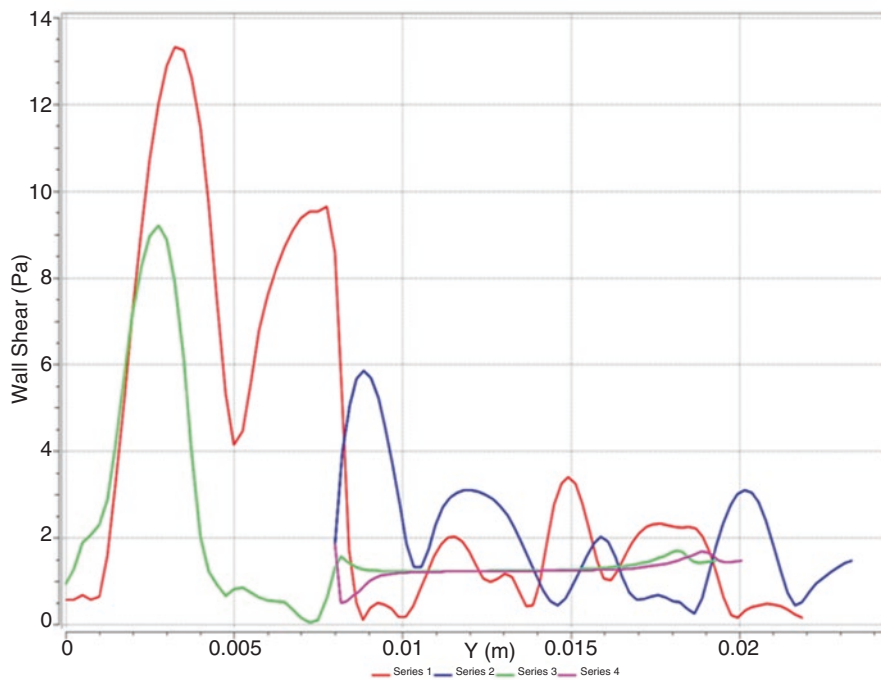**Fig. 21** The velocity streamline and pressure curve for Case 6

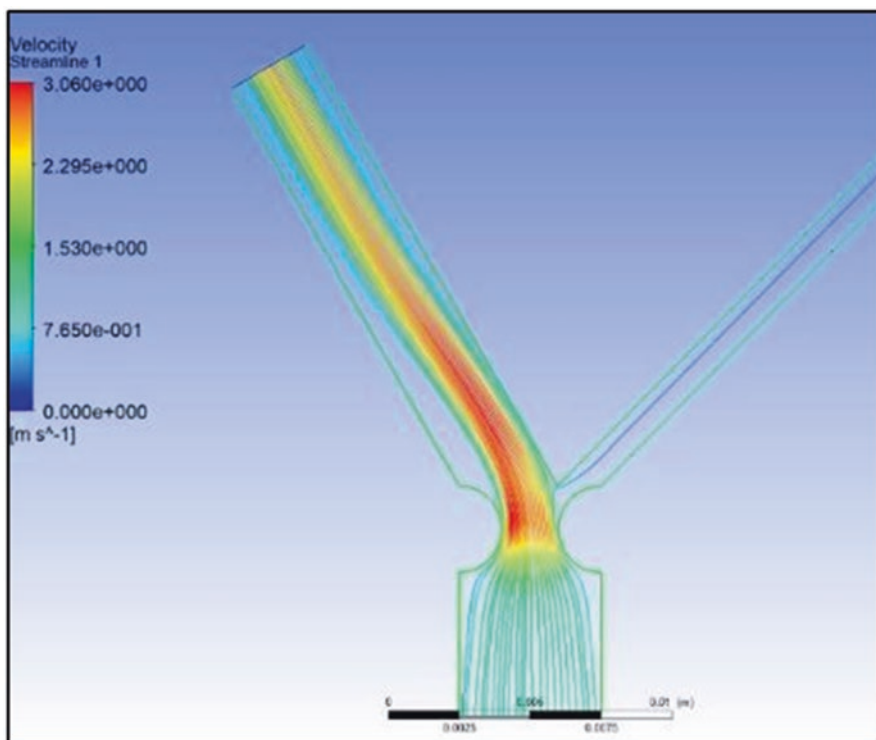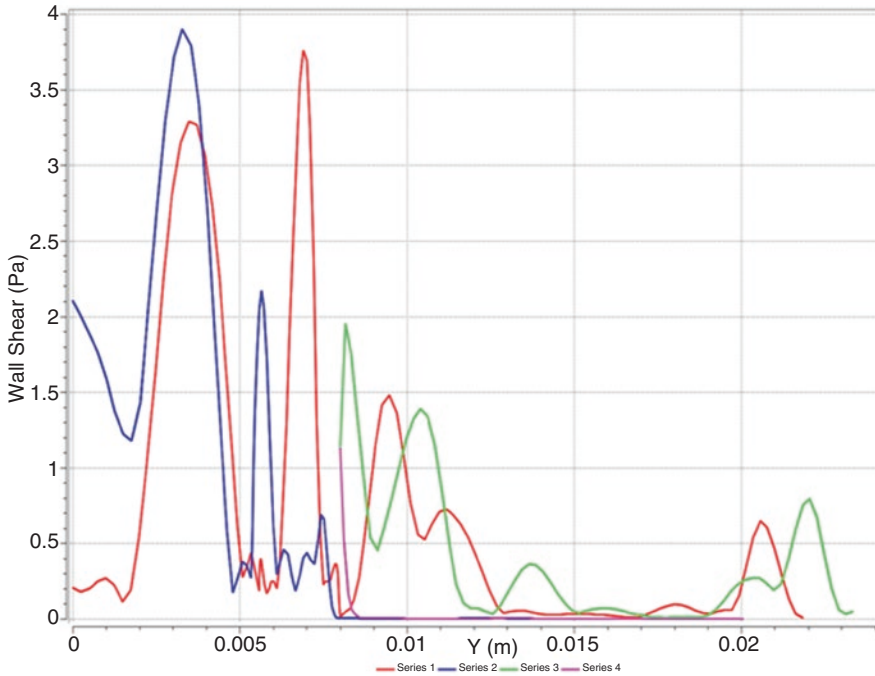**Fig. 22** WSS – various walls for Case 6

Fig. 23 The velocity streamline and pressure curve for Case 7

Fig. 24 WSS – various walls for Case 7

40 Pa and 13 Pa at 0.005 m and 0.0175 m, respectively, whereas the WSS was 30 Pa and 60 Pa at 0.005 m and 0.015 m, respectively. This is the area where a blood clot was introduced as shown in Figs. 25 and 26. The pressure was found to increase at the inlet and decrease towards the outlet.

Case 9: Two plaque configuration 2 with blood clot ($\theta_1 = 30°$, $\theta_2 = 45°$):
This is a similar geometry to Case 4 but with a change in the second angle. The streamline velocity was maximum at 4.507 ms^{-1}. In the left side, there were two changes in the flow directions due the increased velocity and recirculation of blood flow. The velocity in the right stream was high for a while and then it took time for normalizing [12]. The WSS for the left had two peaks at 30 Pa in 0.0125 m and 20 Pa at 0.02 m, whereas for the left, all artery had a peak pressure of 75 Pa at 0.0075 m and it gradually reduced to 60 Pa at 0.01 m and subsequently it decreased to 9 Pa at the outlet, as shown in Figs. 27 and 28. The pressure gradient was high for the inner wall than for the outer wall.

Case 10: Two plaque configuration 2 with blood clot ($\theta_1 = 30°$, $\theta_2 = 45°$):
In this configuration, Case 10 is like Case 5 but with a different angle geometry. Here the velocity was found to be the highest as 7.816 ms-1. There was a huge vortex circulation happening in the left wall away from the bifurcation and plague. Due to the presence of the clot, the velocity was found to increase near the clot in the
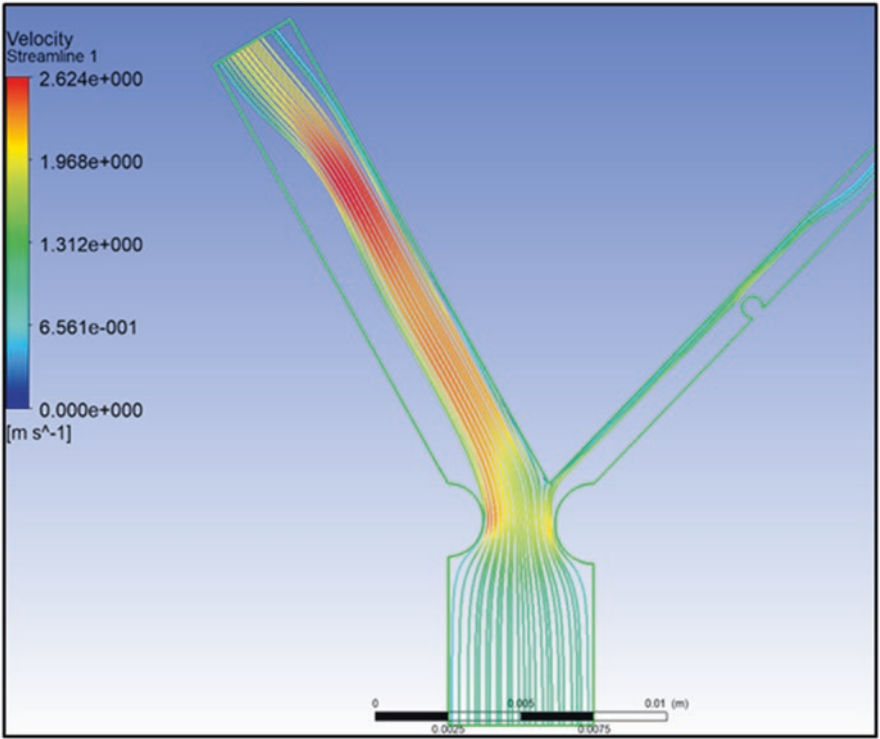
Fig. 25 The velocity streamline and pressure curve for Case 8
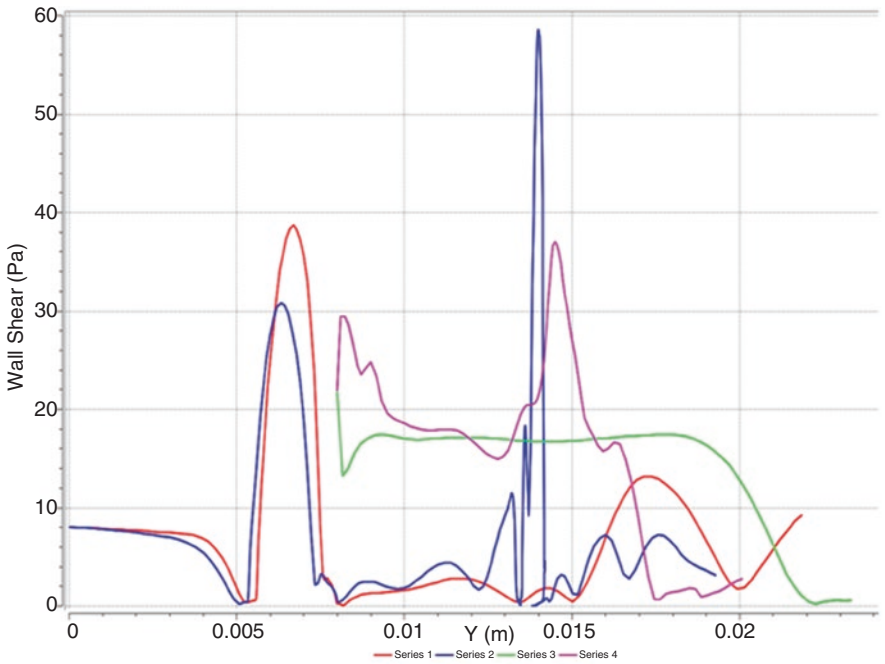
Fig. 26 WSS – various walls for Case 8
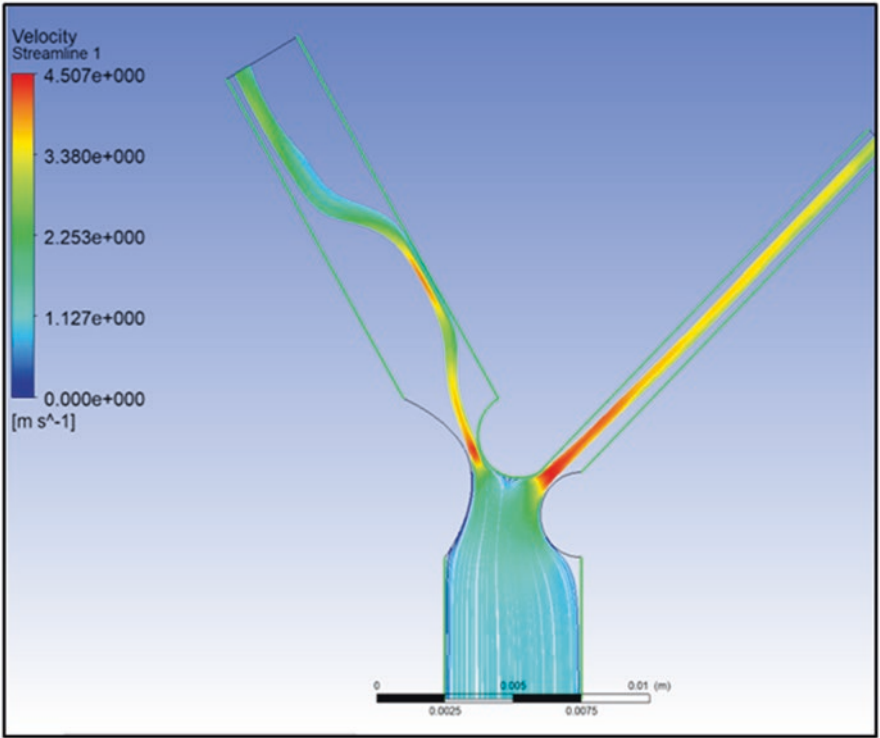
Fig. 27 The velocity streamline and pressure curve for Case 9
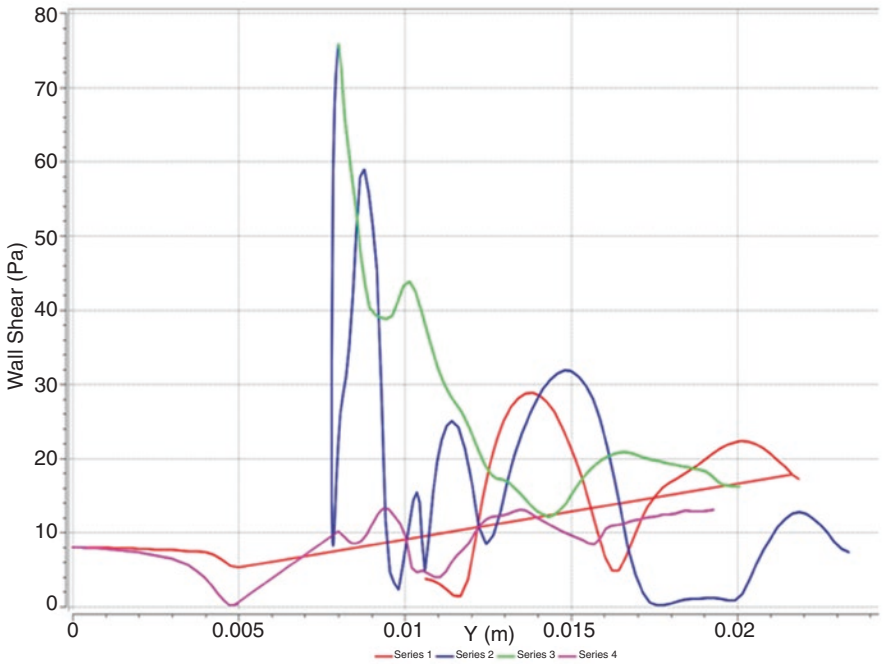
Fig. 28 WSS – various walls for Case 9

right side of the artery. The WSS was increased to 270 Pa at 0.015 m in both the right and left inner wall side as shown in Figs. 29 and 30. The pressure contour was the highest at the left arm of the artery until the clot and then it reduced.

2.2 Hemodynamic Characteristics

This experiment describes the various parameters associated with the hemodynamic characteristics of bifurcated artery with various geometries, plague configuration, and blood clot [10–13].

2.2.1 Blood Flow Velocities Analysis

The streamline velocity measurement performed in computational software for geometric model with rigid walls is shown in Table 2.
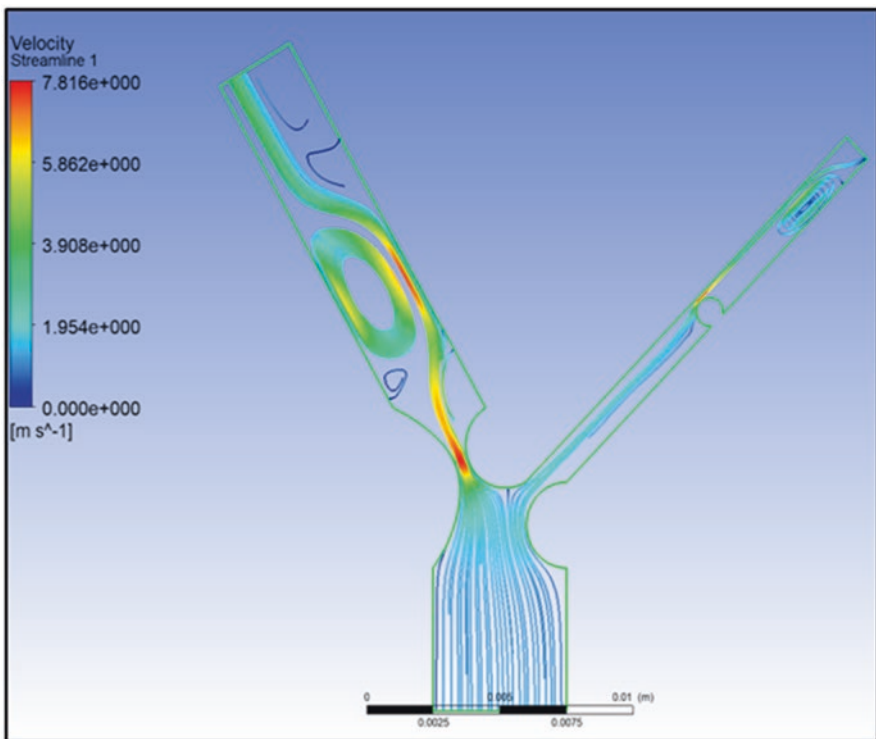
Fig. 29 The velocity streamline and pressure curve for Case 10
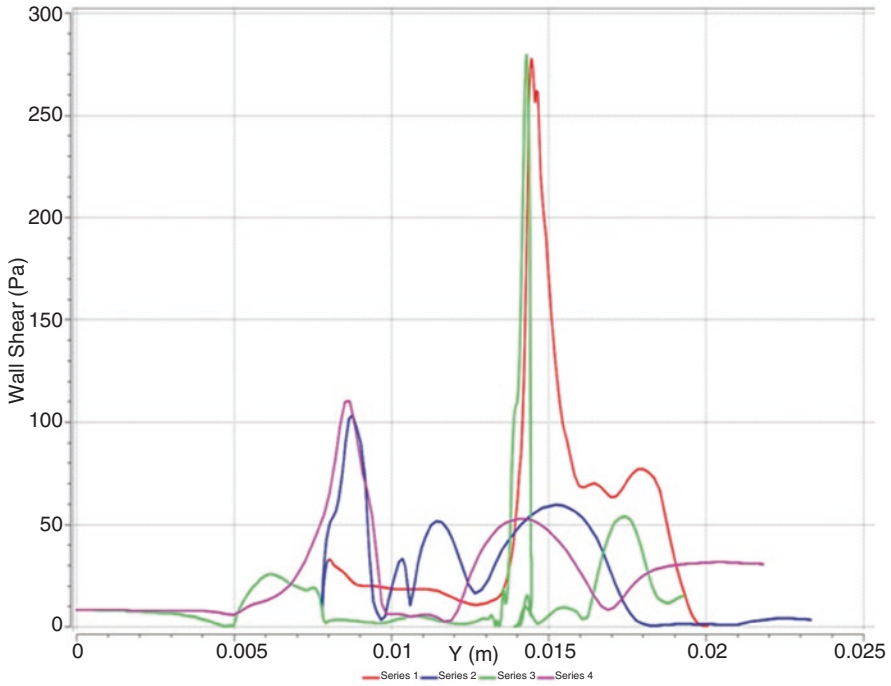
Fig. 30 WSS – various walls for Case 10

Table 2 Velocity streamline for various cases in detail

Geometry	Observation
No plague	High velocity in both walls but in the middle of the streamline not near walls
Plague with configuration 1	Right wall – Recirculation and high velocity towards inner wall rather than middle stream and near the plague Left wall – High velocity near plague
Plague with configuration 1 and blood clot	Right wall – Recirculation and high velocity towards inner wall rather than middle stream but for long distance and near the plague Left wall – Recirculation and high velocity near plague
Plague with configuration 1	Right wall – 2 recirculation near inner and outer wall high velocity near the plague Left wall – High velocity at plague and continued for longer distance.
Plague with configuration 1 and blood clot	Right wall – 2 recirculation near inner and outer wall high velocity near the plague and sides inner wall Left wall – High velocity near the plague

From the graph, it is visible that the velocity increased for each of the cases of 30–30°. But the graph also showed a variation in the velocity for different angles in each case. The 45–45° had a huge velocity variation and increased the value than the 30–30 case. This is because the bifurcation angle changed which in turn changed the secondary flow of various vessel geometries.

The vector analysis was also done, and it was found that at the center of the vessel, the flow is diverted from the left to the right and, at the side walls, it is opposite in direction. Centerline flow is found to be more prominent in the simulations. There is also a significant role of Reynolds number. In this experiment, the Reynolds number was maintained at 400. If the flow velocity at the inlet is changed, then the Reynolds number also changes. For higher Reynolds number, more recirculation at the hooks and the crannies would have an irregular plague wall. At downstream side area, the flow is reversed and the recirculation zone was at its peak. It is twice the diameter in length. In Table 2, the velocity streamline for various cases observed is presented.

As the angle increased, the velocity had a higher value but the same pattern was seen. In both the localities, a distorted low velocity patterns was seen at the external vessel wall, medium velocity values at the sides next to the external wall surface [13].

2.2.2 Wall Shear Stress Analysis

In the central region, the WSS values drop rapidly nearly to zero as the flow of blood suddenly increases in areas. At the zones near recirculation, very low WSS values occur near the sides of the walls. The WSS value is low due to complex flow separation.

The stress value reaching peak at 450 is noted in a 45-degree veins. An increase in blood pressure values is noticed near blocked bifurcated area. A stress value of 70 Pa is observed without clot for $\theta_1 = 30°$, $\theta_2 = 45$ configuration where as a 270 Pa stress value is observed with clot for $\theta_1 = 30°$, $\theta_2 = 45$ configuration as shown in Figs. 31 and 32. The shear stress values purely depend on the shape. Stress values have been reported to be minimum at relation between radius of the vessel and the bifurcation angle. Flow separation is observed at the outer wall near to the bifurcation area and later the flow redevelops and an increase in WSS value is observed.

Although atherosclerotic plaques are preferentially located at bifurcations and inner curves of the vasculature, they co-localize with the regions of low WSS. While high WSS induces an atheroprotective environment, low WSS results in an atheroprone endothelial phenotype; hence, early arterial wall thickening initiates at the regions of low WSS (Table 3).
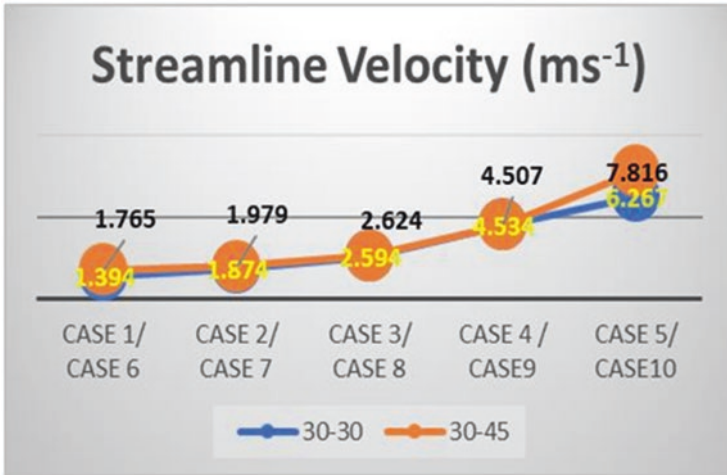
Fig. 31 WSS vs. 30–30 geometry
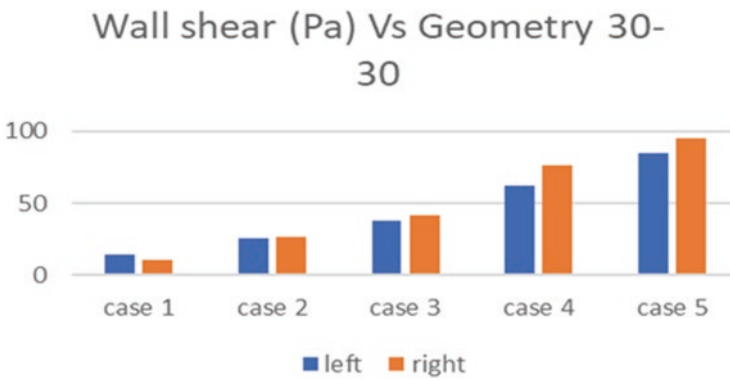
Fig. 32 WSS vs. 30–30 geometry

Table 3 Diameter vs high WSS for each case

Geometry	Distance (mm)	WSS (Pa)	Geometry	Distance (mm)	WSS (Pa)
Case 1	8	10.99	Case 6	3.25	13.32
Case 2	6.43	26.42	Case 7	3.28	3.89
Case 3	15.19	41.46	Case 8	14.01	58.58
Case 4	8	83.22	Case 9	8	75.89
Case 5	15.36	244.75	Case 10	14.31	279.68

2.2.3 Arterial Damage

It is reported that stroke and heart attack are often due to the burst of weak atherma-
nous plaque in the bifurcated arteries. The hemodynamic and the burst of the ste-
notic arteries are still not very clearly understood. The drop in pressure in comparison
with shear stress is higher near the stenosis. Hence, pressure can be a critical trig-
gering factor for the burst of the plague. For the above tables and the figures, it is
evident that high stress in the wall leads to the rupture in Cases 5 and 10. Cases 3
and 7 are also prone to breakage, but the intensity of breakage is more for Cases
5 and 10.

3 Conclusion

Critical factors like velocity curve, WSS, and pressure are studied near the bifur-
cated veins. In the left wall, the flow is highly determined by vortex followed by
strong helical flow. The curvature and asymmetry of the bifurcated profile induces
these types of flow. Very low WSS zones occur at either of the walls. It is observed
that the existence of atherosclerotic plaques is highly related to the vessel profile.
Other important factors for assessing the hemodynamic study of the vessel are
WSS, regions of flow separation, and spilt of unidirectional flow.

References

1. Bernad ES, Bernad SI, Sargan I, Craina ML. Saphenous vein graft patency after geometry remodeling. J Mech Med Biol. 2015;15(06):1540051.
2. Australian Institute of Health, Australian Institute of Health. Australia's health. Australian Government Pub. Service; 2006.
3. Rybicki FJ, Melchionna S, Mitsouras D, Coskun AU, Whitmore AG, Steigner M, Nallamshetty L, Welt FG, Bernaschi M, Borkin M, Sircar J. Prediction of coronary artery plaque progres-sion and potential rupture from 320-detector row prospectively ECG-gated single heart beat CT angiography: lattice Boltzmann evaluation of endothelial shear stress. Int J Cardiovasc Imaging. 2009;25(2):289–99.
4. Shanmugavelayudam SK, Rubenstein DA, Yin W. Effect of geometrical assumptions on numerical modeling of coronary blood flow under normal and disease conditions. J Biomech Eng. 2010;132(6):061004.
5. Johnston BM, Johnston PR, Corney S, Kilpatrick D. Non-Newtonian blood flow in human right coronary arteries: steady state simulations. J Biomech. 2004;37(5):709–20.
6. Soulis JV, Farmakis TM, Giannoglou GD, Louridas GE. Wall shear stress in normal left coro-nary artery tree. J Biomech. 2006;39(4):742–9.
7. Wootton DM, Ku DN. Fluid mechanics of vascular systems, diseases, and thrombosis. Annu Rev Biomed Eng. 1999;1(1):299–329.
8. Mehrabi M, Setayeshi S. Computational fluid dynamics analysis of pulsatile blood flow behav-ior in modelled stenosed vessels with different severities. Math Probl Eng. 2012;1:2012.

9. Harlow FH, Welch JE. Numerical calculation of time-dependent viscous incompressible flow of fluid with free surface. Phys Fluids. 1965;8(12):2182–9.
10. Tu C, Deville M. Pulsatile flow of non-Newtonian fluids through arterial stenoses. J Biomech. 1996;29(7):899–908.
11. Sankar DS, Lee U. Mathematical modeling of pulsatile flow of non-Newtonian fluid in stenosed arteries. Commun Nonlinear Sci Numer Simul. 2009;14(7):2971–81.
12. Chang CC, Atabek HB. The inlet length for oscillatory flow and its effects on the determination of the rate of flow in arteries. Phys Med Biol. 1961;6(2):303.
13. Chandran KB, Mun JH, Choi KK, Chen JS, Hamilton A, Nagaraj A, McPherson DD. A method for in-vivo analysis for regional arterial wall material property alterations with atherosclerosis: preliminary results. Med Eng Phys. 2003;25(4):289–98.